Global Biogeochemical Cycles

RESEARCH ARTICLE
10.1029/2020GB006888

Key Points:

- This is the most comprehensive global analysis of reservoir methane and CO_2 emissions to-date, and the first to estimate methane degassing
- Although diffusive CH_4 fluxes are somewhat lower than previously believed, CH_4 fluxes via degassing and ebullition are much larger
- The highest reservoir greenhouse gas emissions globally occur in the tropics and subtropics, with CH_4 degassing and ebullition as dominant flux paths

Supporting Information:

Supporting Information may be found in the online version of this article.

Correspondence to:

J. A. Harrison,
john_harrison@wsu.edu

Citation:

Harrison, J. A., Prairie, Y. T., Mercier-Blais, S., & Soued, C. (2021). Year-2020 global distribution and pathways of reservoir methane and carbon dioxide emissions according to the greenhouse gas from reservoirs (G-res) model. *Global Biogeochemical Cycles*, *35*, e2020GB006888. https://doi.org/10.1029/2020GB006888

Received 13 NOV 2020
Accepted 14 MAY 2021

Year-2020 Global Distribution and Pathways of Reservoir Methane and Carbon Dioxide Emissions According to the Greenhouse Gas From Reservoirs (G-res) Model

John A. Harrison[1], Yves T. Prairie[2], Sara Mercier-Blais[2], and Cynthia Soued[2]

[1]School of the Environment, Washington State University, Vancouver, WA, USA, [2]Department of Biological Sciences, University of Quebec at Montreal (UQAM), Montréal, QC, Canada

Abstract Collectively, reservoirs constitute a significant global source of C-based greenhouse gases (GHGs). Yet, global estimates of reservoir carbon dioxide (CO_2) and methane (CH_4) emissions remain uncertain, varying more than four-fold in recent analyses. Here we present results from a global application of the Greenhouse Gas from Reservoirs (G-res) model wherein we estimate per-area and per-reservoir CO_2 and CH_4 fluxes, by specific flux pathway and in a spatially and temporally explicit manner, as a function of reservoir characteristics. We show: (a) CH_4 fluxes via degassing and ebullition are much larger than previously recognized and diffusive CH_4 fluxes are lower than previously estimated, while CO_2 emissions are similar to those reported in past work; (b) per-area reservoir GHG fluxes are >29% higher than suggested by previous studies, due in large part to our novel inclusion of the degassing flux in our global estimate; (c) CO_2 flux is the dominant emissions pathway in boreal regions and CH_4 degassing and ebullition are dominant in tropical and subtropical regions, with the highest overall reservoir GHG fluxes in the tropics and subtropics; and (d) reservoir GHG fluxes are quite sensitive to input parameters that are both poorly constrained and likely to be strongly influenced by climate change in coming decades (parameters such as temperature and littoral area, where the latter may be expanded by deepening thermoclines expected to accompany warming surface waters). Together these results highlight a critical need to both better understand climate-related drivers of GHG emission and to better quantify GHG emissions via CH_4 ebullition and degassing.

Plain Language Summary By damming rivers, humans have created millions of reservoirs, which, collectively, constitute an important greenhouse gas source, especially for methane, a particularly potent greenhouse gas. Using observed relationships between reservoir characteristics and greenhouse gas emissions, we show that much more methane either bubbles out of reservoirs or is emitted just downstream from reservoirs than was previously known. This is important because it may be possible to reduce methane emissions from downstream of reservoirs by selectively withdrawing water from near the surface of reservoirs, which tends to be methane-poor, rather than from greater depths, where methane often accumulates. We also found that on a per-area basis reservoirs are a more potent source of greenhouse gases than previously recognized, and that the highest rates of emissions occur in the tropics and subtropics. Finally, we show that estimates of reservoir greenhouse gas emissions are quite sensitive to climate-related factors like temperature.

1. Introduction

Recent work has highlighted the importance of inland waters generally, and reservoirs specifically, as hotspots for carbon processing and C-based greenhouse gas (GHG) emission (Butman & Raymond, 2011; Cole et al., 2007; Deemer et al., 2016; Deemer & Holgerson, 2021; DelSontro et al., 2018; Maavara et al., 2017, 2020; Raymond et al., 2013; Rosentreter et al., 2021; Tranvik et al., 2009). Yet, global estimates of reservoir GHG emissions remain highly uncertain, varying by more than four-fold (range: 741–3,380 Tg CO_2 equivalents yr^{-1}) in recent analyses (Barros et al., 2011; Bastviken et al., 2011; Deemer et al., 2016; Hertwich, 2013; St. Louis et al., 2000; Rosentreter et al., 2021).

To date, global estimates of reservoir GHG emissions have been derived simply by multiplying global reservoir surface area by emission rates averaged from a limited, but growing, set of in situ flux measurements. While this approach may provide a reasonable first-order approximation of global fluxes, the accuracy of

such a method relies upon a number of assumptions, all of which may have a large but heretofore unknown and largely unexplored impact on global flux estimates. Notably, the generally applied approach implicitly assumes that sampling of reservoirs accurately reflects the existing age distribution of reservoirs (because GHG emissions from reservoirs tend to decline over time [Abril et al., 2005; Teodoru et al., 2012]). It also implicitly assumes that sampling adequately captures and represents the natural spatial variation in GHG flux rates both within and between reservoirs, and temporal variation over seasonal to multi-year scales, all of which are often substantial, necessitating adequate spatial and temporal coverage of measurements (Wik et al., 2013, 2016). The importance of such assumptions to estimates of aquatic GHG fluxes at large-scales is, to-date, largely unknown and untested. In addition, due to the lack of any continentally or globally applicable models for predicting aquatic GHG fluxes, it has not been possible to estimate the geographic distribution of reservoir GHG fluxes at the global scale beyond broad generalizations about latitudinal patterns (e.g., Deemer et al., 2016). Nor have spatial distributions of various flux pathways for CH_4 been quantified or evaluated at large scales. In fact, efforts to estimate reservoir GHG fluxes have generally focused solely on diffusive gas fluxes (Barros et al., 2011; St. Louis et al., 2000), and it is only recently that ebullition fluxes have been incorporated into global reservoir GHG flux estimates (Deemer et al., 2016; delSontro et al., 2018). It has been shown that CH_4 emissions due to turbine degassing can be the dominant pathway in individual reservoirs (Abril et al., 2005; Soued & Prairie, 2020) and could therefore be substantial at the global scale, but these fluxes have not previously been estimated (Deemer et al., 2016).

In previous work, we reported on the development of the G-res model, which is an open and globally consistent predictive framework for estimating the anthropogenic GHG footprint of individual reservoirs (Prairie et al., 2017, 2018). Here, our main objective is to apply the underlying emission models of G-res to provide the first-ever spatially and temporally explicit global estimate of reservoir CO_2 and CH_4 fluxes and the first-ever global estimate of reservoir degassing fluxes. In addition, we explore the relative contribution of the various emission pathways and how they vary across regions of the world. Lastly, we conducted efficiency and sensitivity analysis of the models to help identify important research needs and facilitate better estimates of global and regional GHG emissions from reservoirs going forward.

2. Methods

2.1. Overview

Broadly, our approach to developing a spatially explicit estimate of the global GHG flux from reservoirs involved three steps: (a) extraction of information required to apply G-res models to a larger set of reservoirs using globally consistent GIS layers, (b) application of the predictive models globally, including estimates of associated uncertainty, and (c) assessment of model sensitivity and efficiency in order to understand how changes in drivers are likely to affect global GHG fluxes and to identify especially important and promising avenues for additional research and refinement. The development of the emission models is described in detail in publicly available model documentation (Prairie et al., 2017), and model equations, a description of model input datasets, and model calibration and validation data are provided in Tables S1 and S2, and in a downloadable data set (Prairie et al., 2021), respectively. However, the models are described briefly below for completeness (Sections 2.2 and 2.3), and steps 2 and 3 are described in Sections 2.4 and 2.5.

2.2. Model Development/Calibration Data Set

Using data compiled from 223 globally distributed reservoirs for which published measurements were available (Figure 1, Prairie et al., 2021), the G-res framework was developed from multiple linear regression models to predict per-area and per-reservoir CO_2 and CH_4 emissions. Prior to regression analysis, per-area flux estimates were processed in several ways to improve internal consistency. First, flux measurements were annualized to account for the fact that measurements are often made during summer months when fluxes might be higher than at other times of the year. Briefly, this annualization was accomplished for literature-reported diffusive fluxes of CO_2 and CH_4, and CH_4 bubbling fluxes by combining the mean monthly air temperature for the month(s) in which fluxes were measured with the known temperature dependencies for CO_2 and CH_4 production ($Q_{10} = 2$, and 4 for CO_2 and CH_4, respectively [Inglett et al., 2012; Yvon-Durocher et al., 2014]), and averaging flux estimates across all 12 months in a year to achieve an annual flux rate.

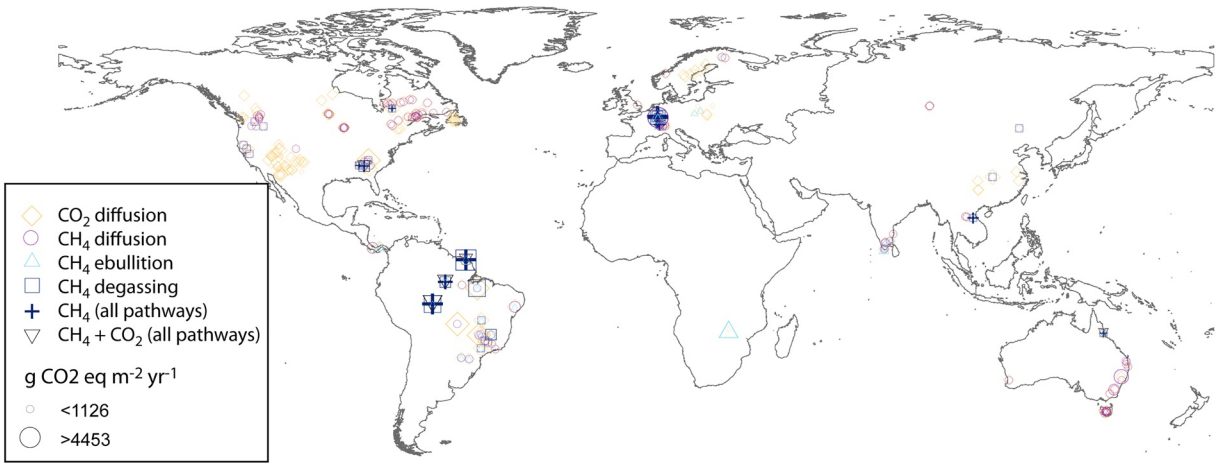

Figure 1. Locations of greenhouse gas flux measurements used to develop G-res submodels; symbols represent the pathway for which flux estimates were available and the size of each symbol is proportional to the estimated flux rate (g CO_2 eq. m^{-2} yr^{-1}).

This process was carried out for each reservoir. In addition, when direct CH_4 ebullition data were only available from littoral sites within reservoirs (17 of the reservoirs used to develop the G-res ebullition model), we accounted for the fact that bubbling tends to decline with increasing water column depth (due to increased hydrostatic pressure) by multiplying littoral ebullition rates by the ratio of littoral: total reservoir area to achieve reservoir-wide estimates. The extent of littoral area used was either the littoral area reported in the original publication (used when available) or the littoral area estimated using the maximum depth sampled for ebullition provided in the original publication (used when a direct estimate of littoral area was not available). Although this approach may underestimate lake-wide ebullition fluxes of CH_4 in some systems, we view it as an improvement over the historical approach, which simply assumes that these littoral flux rates are representative of whole-lake fluxes, thereby potentially overstating their importance. Once annualized and area-corrected, flux estimates were $\log_{10}$ transformed in order to achieve approximate normal distribution of fluxes. For CH_4 degassing emissions, the empirical model uses the change in concentration between the water intake depth and directly out of the outlet as the predicted response variable.

In addition to pre-processing flux measurements, we also collected information on reservoirs and associated catchment characteristics likely to influence CO_2 and CH_4 production and emission from a variety of sources. These potential drivers are described in detail in Prairie et al. (2017, 2018). Briefly, they included reservoir characteristics such as latitude, surface area, volume, maximum depth, mean depth, littoral area (defined as area with depth less than 3 m) as a fraction of total lake area, water residence time, mean monthly and annual air temperature, mean annual wind speed, mean global horizontal irradiance, estimated phosphorus loading and concentration, soil carbon content prior to flooding and catchment characteristics such as catchment area, annual precipitation, mean annual runoff, population density, annual reservoir inflow, and catchment land cover (Prairie et al., 2017). When possible, these data were taken directly from peer-reviewed studies of reservoirs, but when it was not possible to mine primary literature for reservoir or catchment characteristics, we relied on attributes provided by the Global Reservoirs and Lakes (GRanD) database (Lehner et al., 2011) or from published GIS coverages (Prairie et al., 2017, 2021). In some cases (notably average depth, thermocline depth, littoral area, water residence time, and phosphorus concentrations) we estimated values using peer-reviewed approaches (Prairie et al., 2017). Model selection was determined based on best fit, reasonableness (i.e., drivers had to have a reasonable biophysical explanation to be included), and global availability of model drivers. Flux estimates from 107, 102, 27, and 38 reservoirs were used to develop CO_2 diffusion, CH_4 diffusion, CH_4 ebullition, and CH_4 degassing models, respectively (Figure 1, Prairie et al., 2021). In a subset of reservoirs, flux estimates were available from multiple years, such that a total of 169, 160, 46, and 38 individual flux estimates were used to develop the CO_2 diffusion, CH_4 diffusion, CH_4 ebullition, and CH_4 degassing models, respectively. Significant input parameters ($P < 0.05$ by multiple linear regression) for each GHG flux pathway are listed in Table 1, and complete models and model input variables are included in Tables S1 and S2, respectively. Whereas diffusive and ebullitive flux models

Table 1
Influence of Each Input Parameter on the Four Pathways Estimated by the G-res Model

	CO_2 diffusion	CH_4 diffusion	CH_4 ebullition	CH_4 degassing
Age	−	−		
Temperature	+	+		
Soil C content	+			
Total phosphorus	+			
Reservoir area	+			
% Littoral area		+	+	
Cumulative radiance [a]			+	
Hypolimnetic release (Y/N)				x
Water residence time				+
Diffusive CH_4 emissions				+

[a]Cumulative radiance is estimated as the mean global horizontal radiance for the ice-free period multiplied by the number of ice-free months.

Notes. Minus (−) or plus (+) signs indicate a negative or positive relationship between the emission pathway and the parameter respectively. "x" indicates a binary decision whether to include a given reservoir in the global total based on its characteristics. See Table S1 for model equations, Table S2 for coefficient definitions and values, Prairie et al. (2021) for flux estimates used in model development and evaluation, and Prairie et al. (2017) for a more complete description of the models and their development.

were developed using per-area flux measurements, the degassing sub-model was developed to predict the difference in CH_4 concentrations upstream and downstream of dams. When multiplied by water flow and divided by a reservoir's surface area, this concentration difference was considered the per-area degassing flux of CH_4.

2.3. Emission Pathway Sub-Models

Each emission pathway (CO_2 diffusion, CH_4 diffusion, ebullition, and degassing) was modeled as a multivariate relationship between the annualized per-area emission rates and potential predictor variables described above, following suitable transformation. Flux rates are reported in units of CO_2 equivalents, assuming a per-mass 100-year warming potential for CH_4 34-fold that of CO_2 (IPCC 2013). Variable selection was carried out through the elastic net regression procedure which is particularly well-suited to "short and fat" datasets (small number of observations relative to the number of potential predictors) with colinear predictor variables. The exact form of the resulting models is described in more detail in publicly available G-res documentation (Prairie et al., 2017, 2021) but the variables retained, the sign of their coefficients and their relative importance are summarized for each sub-model in Table 1. For completeness, the sub-model equations (G-res V.3) and variable definitions are reproduced in Supplementary Material (Tables S1 & S2). In order to facilitate attribution of reservoir GHG fluxes, G-res partitions CO_2 flux from each reservoir into anthropogenic and non-anthropogenic fractions. For the purpose of this global GHG flux estimation and comparison with previous estimates, we report here only total CO_2 emissions. Similarly, the G-res framework estimates the degassing pathway only for reservoirs with deep water intakes (deeper than the thermocline), where CH_4 can accumulate to very high concentrations. Information on water intake depth was largely unavailable. However, due to the greater operational flexibility it offers, the deep-water withdrawal configuration is known to be more common among hydropower reservoirs. Thus, we used this (hydroelectricity as a reported usage in the GRanD database) as a criterion to consider degassing in the modeled emissions of a given reservoir. This assumption is clearly a simplification of reality, since deep water intake is neither systematic in, nor limited to, hydropower reservoirs. However, it remains the most sensible approach for a first-order estimate of degassing on a global scale given currently available information. Hydroelectricity was a reported use for 33.7% of the reservoirs in our global reservoir database, but these reservoirs tended to be large, such that cumulatively they accounted for 83% of the total global reservoir surface area.

2.4. Spatial Extrapolation

G-res submodels were applied to 4,563 reservoirs either in the GRanD database with the necessary driver data available (Lehner et al., 2011) or added by us (164 reservoirs). These reservoirs had a worldwide distribution and collectively represent 68% of estimated global reservoir surface area. The four largest reservoirs in the GRanD database (Lakes Victoria, Baikal, Ontario, and Onega) collectively occupy more than 128,000 km^2. As these systems are large natural lakes where damming has resulted in negligible increases in surface area and depth, these large lakes were excluded from our global estimate of reservoir GHG fluxes. The GRanD database underestimates the surface area of small reservoirs since it is a compilation of the world largest reservoirs (reservoirs exceeding 0.1 Mm^3 in volumetric capacity). Because the G-res database used in this analysis (Prairie et al., 2021) relies heavily upon the GRanD database, it was subject to this same limitation. The extent of this underestimation is difficult to assess, but can be examined using the approach developed by Downing et al. (2006) and applied by others (e.g., Lehner et al., 2011), which relies on the statistical properties of a canonical set of reservoirs, extrapolated to a reasonable lower size limit. Using this approach, and discounting the four large lakes, yielded an estimated total global surface area for all reservoirs greater than 0.1 km^2, of approximately 350,000 km^2 (comprised of 87,800 reservoirs), which is close to estimates used in other recent global analyses (e.g., Deemer et al., 2016). To account for the difference in surface area between reservoirs represented in the G-res database and our estimated global total, we multiplied the total global fluxes from G-res database reservoirs by a factor of 1.47 (the ratio between an estimated global reservoir surface area of 350,000 km^2 and the total surface area of reservoirs globally for which it was possible to use G-res to calculate all four G-res-estimated GHG flux pathways) to attain global flux estimates, and we distributed additional GHG fluxes spatially in proportion to the occurrence of the G-res database reservoir surface area. As noted above, following a necessary, albeit oversimplifying, assumption that only hydroelectric reservoirs have deep water intakes, we calculated a degassing flux only for those systems.

2.5. Estimating Global Total Gas Fluxes and Associated Uncertainty

To avoid influence of extreme outliers on error estimates, we removed outliers using Cook's distance (criterion for removal: Cook's distance >3*μ; Cook 1977). This resulted in removal of 3, 15, 3, and 2 reservoirs from G-res CO_2 diffusion, CH_4 diffusion, CH_4 ebullition, and CH_4 degassing models, respectively. To correct for bias associated with developing models using log-transformed data (Newman, 1993), we calculated regression standard error of residuals (s) as $\sqrt{\frac{\Sigma\left(y_i - \hat{y}_i\right)^2}{\mathrm{DF}}}$, where y_i is model-predicted flux, $\hat{y}_i$ is measured flux, and *DF* is the number of degrees of freedom (number of available comparisons between measurements and model predictions minus the number of calibrated parameters in each G-res sub-model). We then ran a Monte Carlo analysis in which all model estimates were amended with a randomly determined error (with a Gaussian distribution and a mean equal to the standard error of residuals (s, defined above). Predicted per-reservoir fluxes were subsequently exponentiated and summed. This calculation was repeated 1,000 times with random assignment of errors and the median and 95% confidence interval values for predicted global total fluxes were determined based on distribution of results. Median values resulting from this exercise are presented as the most probable estimate (i.e., highest probability density) of global reservoir fluxes. This approach to propagating the uncertainty for each flux pathway model to estimate the global GHG footprint means that greater model uncertainty results in higher estimated global flux. This effect is not negligible. In the case of G-res models, the estimated global flux accounting for the uncertainty in the prediction of each individual reservoir was 1.48, 1.99, 4.45, and 4.88-fold higher than uncorrected totals for CO_2 diffusion, CH_4 diffusion, CH_4 degassing and CH_4 ebullition sub-models, respectively.

Fluxes reported by latitudinal region were binned into boreal, temperate, subtropical, and tropical regions, defined as >62°N and S, 35–62°N and S, 23.5–35°N and S, and <23.5°N and S, respectively. Fluxes were also binned and summed by climate zone, as defined by the IPCC (Rubel & Kottek, 2010). Climate zones used for this exercise were: boreal, cool temperate, temperate warm/dry, temperate warm/moist, tropical dry/montane, and tropical moist/wet. Unless specified as climate-related (e.g., in Table 5), the terms boreal, temperate, and tropical refer to latitudinal regions.

Table 2
Performance Statistics for G-res Submodels, Including Nash Sutcliffe Efficiency (NSE) Values for Both Per-Area and Per-Reservoir Predictions, Median and Interquartile Range Values for Percent Error for the Models, and the Number of Flux Estimates Used to Develop and Evaluate the Models

Flux pathway	NSE Per-area	NSE Per-reservoir	Median % Error (IQR)	n	Outliers
CO_2 Diffusion	0.37	0.89	11 (−44–52)	169	3
CH_4 Diffusion	0.52	0.84	−21 (−54–121)	160	15
CH_4 Degassing	0.57	0.74	21 (−76–187)	38	2
CH_4 Ebullition	0.29	0.58	14 (−84–318)	46	3

Notes. The number of outliers excluded from NSE and IQR calculations are also reported. See methods (Section 2.8) for description of the method used to exclude outliers.

2.6. Model Sensitivity and Efficiency Analyses

To evaluate G-res sensitivity to input data and model parameters, we sequentially increased individual model input parameters by 10% and evaluated the resulting change in model predictions. To evaluate the importance of G-res model components, we performed an efficiency analysis (as described in Nash & Sutcliffe, 1970), wherein model components were removed one at a time and the resulting change in Nash Sutcliffe Efficiency (NSE) was evaluated. NSE is a measure of model skill where (similar to r^2) a value of 1 connotes perfect model predictions but where a value of zero indicates that a mean of measurements is as good a predictor of measurements as the model being evaluated, and negative values indicate that a model's predictions do worse than simply using the mean of available measurements (Nash & Sutcliffe, 1970).

3. Results and Discussion

3.1. Model Performance

Although error associated with CO_2 and CH_4 flux predictions for individual reservoirs was, in some cases, substantial (e.g., see Table 2 and Figure 2), each of the individual G-res submodels was reasonably proficient at predicting spatial variation in per-area fluxes, and, more importantly for this global analysis, performed well in predicting per-reservoir fluxes (NSE > 0.8 for CO_2 and CH_4 diffusion, and NSE > 0.5 for CH_4 ebullition and degassing, Table 2, Figure 2). Further, the G-res submodels were bias-free in that slopes of least squares linear regressions between measured and model-estimated fluxes were not significantly different from unity for any of the G-res submodels (Figure 1). Submodels also performed well when outputs from more than one submodel were summed and compared with summed measurements from several systems (NSE: 0.71 and 0.83 for total CH_4 and Total C-based greenhouse gases, respectively). These comparisons were also free of apparent bias (Figure 2). G-res submodels were somewhat less skilled at predicting per-area fluxes than per-reservoir fluxes, but still performed better than an average of measurements in predicting per-area CO_2 and CH_4 fluxes, as indicated by positive NSE values (≥0.29 in all submodels, Table 2).

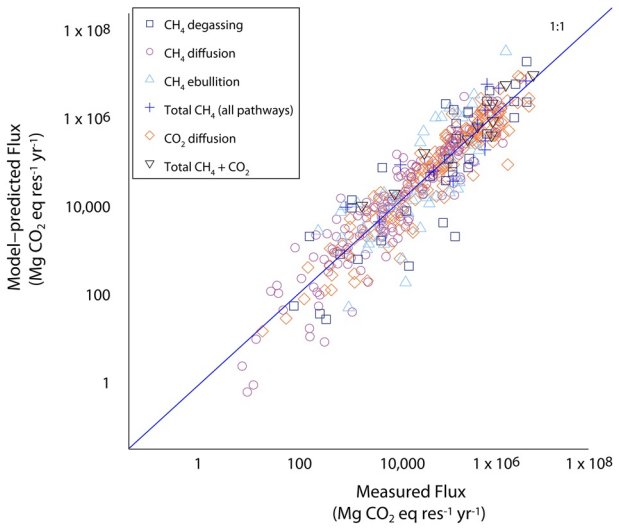

Figure 2. G-res predicted CH_4 and CO_2 fluxes (Mg CO_2 eq reservoir^{-1} yr^{-1}) by pathway versus measurements. Nash Sutcliffe Efficiency values for G-res submodels (each flux pathway) are shown in Table 2.

3.2. Global CO_2 and CH_4 Fluxes

Using G-res, we estimate global flux of GHGs from reservoirs as 1,076 Tg CO_2 eq. yr^{-1} (range: 730–2,412 Tg CO_2 eq. yr^{-1}) mainly as CH_4 (328 and 748 Tg CO_2 eq. yr^{-1} for CO_2 and CH_4, respectively). For methane, our estimate of diffusive plus ebullitive CH_4 emission (337 Tg CO_2 eq. yr^{-1}) is similar to that of Hertwich et al. (2013), and more than double that of Bastviken et al. (2011), but somewhat smaller than other recent global estimates, which are based on averages of reported fluxes and range from 606–2,380 Tg CO_2 eq. yr^{-1} (Table 3). Degassing fluxes of CH_4, which have not been accounted for in other global analyses, were the largest and also the most uncertain flux in our estimate, accounting for 411 Tg CO_2 eq. yr^{-1} (95% confidence range: 227–1,261 Tg CO_2 eq. yr^{-1}). When degassing is included, our median global estimate of reservoir greenhouse gas fluxes (Tg CO_2 eq. for CO_2 plus CH_4) is among the largest that have been reported, and is 45% higher than a recent estimate by Deemer et al. (2016). G-res-estimated average global per-area GHG emissions (Tg CO_2 eq. km^{-2} of reservoir surface area) are the highest that have been reported, exceeding those of Deemer et al. (2016) and St. Louis et al. (2000), by 29% and 36%, respectively.

Globally, we estimate that diffusive CH_4 fluxes from reservoirs, which, of all CH_4 flux pathways, have received the most attention to-date, are

Table 3
Global Reservoir, Year-2020 Fluxes of CO_2 and CH_4 From This Study and Other Recent Analyses

	Global reservoir area used (10^3 km^2)	CO_2 (Tg CO_2 eq yr^{-1})	CH_4 (Tg CO_2 eq yr^{-1})	$CO_2 + CH_4$ (Tg CO_2 eq yr^{-1})	$CO_2 + CH_4$ (Mg CO_2 eq km^{-2} yr^{-1})
This study	350	328 (276–414)	748 (454–1,998)	1,076 (730–2,412)	3,074 (2,086–6,891)
This study (no degassing)	350	328 (276–414)	337 (227–737)	664 (503–1,151)	1,897 (1,437–3,289)
Deemer et al. (2016)	311	135	606	741	2,383
Hertwich (2013)	330	279	331	610	1,815
Bastviken et al. (2011)	340		136		400
Barros et al. (2011)	500	176	680	856	1,712
St-Louis et al. (2000)	1,500	1,000	2,380	3,380	2,253

Notes. All values have been converted to mass CO_2 eq. yr^{-1} using a 100-year greenhouse warming potential factor of 34 for CH_4. Ranges in parentheses represent 95% confidence intervals for G-res v3 estimates. Differences between studies in total estimated global reservoir surface area generally result from differences in statistical methods for estimating the cumulative surface area of small reservoirs. In some cases total CH_4 fluxes differ slightly from sums of individual flux pathways due to rounding.

small relative to other reservoir GHG flux pathways, accounting for just 7% of the total CH_4 flux and 5% of the greenhouse effect due to combined CH_4 plus CO_2 flux. In contrast, ebullition and, especially, degassing fluxes are comparatively large, accounting for 38% and 55% of the global total CH_4 flux, respectively. Overall, diffusive fluxes of CO_2 are substantial, accounting for almost one third (30.5%) of the greenhouse liability from reservoirs, but exert a smaller impact on greenhouse warming than reservoir-sourced CH_4, which collectively accounts for 69.5% of the greenhouse warming effect due to reservoir emissions globally. This fraction would be substantially greater if a less conservative greenhouse warming potential were used for CH_4. If, for example, we used the 20-year greenhouse warming potential (85, IPCC 2013) for CH_4 instead of a 100-year greenhouse warming potential, CH_4 would constitute 85% of total annual warming potential emitted from reservoirs. In addition, whereas virtually all of the CH_4 emitted from reservoirs can be considered anthropogenic, a substantial portion of the global CO_2 flux can be considered non-anthropogenic in origin as ~69% of these emissions would have occurred even in the absence of reservoir construction (Prairie et al., 2017).

Although this analysis revises the estimate of global total diffusive CH_4 flux and ebullitive CH_4 flux downward relative to other recent studies (Table 3), the total estimated global flux of CH_4 (22.0 Tg y^{-1}; range: 13.4–58.8 Tg CH_4 y^{-1}) we report is higher than that estimated by other recent efforts (Table 3). This is due, in large part, to our novel inclusion of CH_4 degassing in this global estimate of reservoir GHG fluxes. G-res per-area estimates of CH_4 diffusion are lower than past estimates because the G-res models attempt to account for potential sampling bias associated with reported flux measurements. Reasons that past estimates of global diffusive CH_4 fluxes, and global ebullitive CH_4 fluxes may have been overestimated include: disproportionate sampling of high-emission reservoirs, seasonal sampling that focuses on summer conditions (which tend to foster large GHG fluxes), inappropriate temporal averaging that neglects winter ice cover, use of littoral only emissions to represent emissions from the total surface area of reservoirs, and oversampling of highly active regions within reservoirs. In the formulation of G-res models, every effort was taken to account for these potential sources of bias in the measurement data. For example, measurements of CH_4 and CO_2 diffusion used in model calibration were temperature-corrected to account for potential seasonal bias in sampling, and ebullitive emissions during ice-covered months (i.e., months with mean air temperatures <0°C) were assumed to be zero while diffusive emissions were assumed to be emitted at ice-off after proceeding under 4°C conditions during the ice-covered period. Although sensible, these assumptions remain largely unverified by field observations and might still overestimate CH_4 diffusive flux, as a portion of the CH_4 produced under ice can be oxidized before ice-off. However, we argue that these modeling assumptions represent an improvement over simply extrapolating ice-free period fluxes to the whole year. These efforts resulted in comparatively low annual estimates of global diffusive CH_4 fluxes and CH_4 ebullition fluxes. However, the addition of CH_4 degassing, arguably a less certain flux (due to modeling assumptions and fewer data points), more than compensated for lower estimates of other CO_2 and CH_4 fluxes, leading to an estimate of global reservoir CH_4 fluxes that is similar to, or greater than, other recent estimates (Table 3) and

comparable to other major global anthropogenic CH_4 sources such as landfills, biomass burning, and rice paddies (68, 29, and 30 Tg CH_4 y^{-1}, respectively; Saunois et al., 2020). We estimate that collectively reservoirs account for ~6% (range: 3.7%–17.4%) of total global anthropogenic CH_4 emissions (340–381 Tg CH_4 y^{-1}) and ~14% (range: 7.1%–50.4%) of total global freshwater CH_4 emissions (Saunois et al., 2020).

The likely global importance of CH_4 degassing is also interesting from a GHG management perspective as it suggests some potential to limit or reduce reservoir CH_4 emissions. G-res output suggests that if all reservoir CH_4 degassing were eliminated, global GHG fluxes from reservoirs would be reduced by 31%–52%. Because high degassing fluxes are most likely to occur when water is drawn through a dam from a reservoir's hypolimnion, where low-O_2 conditions allow CH_4 to accumulate, constructing dams that draw water from well-oxygenated near surface portions of a reservoir's water column or managing water withdrawals to minimize release of hypolimnetic waters could substantially reduce downstream degassing CH_4 fluxes. For example, a simulated increase in water withdrawal depth by as little as 3 m (from the hypolimnion to the metalimnion) yielded a 92% reduction in CH_4 degassing emissions from a Malaysian reservoir (Batang Ai) (Soued & Prairie, 2020). It is also possible that retrofitting existing dams with epilimnetic water withdrawal structures or hypolimnetic aeration systems could reduce downstream degassing, while also likely mitigating other environmental impacts of dams on downstream ecosystems (Michie et al., 2020). While the effectiveness, costs, and potential tradeoffs associated with these solutions are not yet documented, they certainly deserve further attention and study.

3.3. Spatial Distribution of Reservoir GHG Fluxes

G-res allows a first-ever analysis of the global distribution of reservoir greenhouse gas fluxes that takes into account characteristics of reservoirs beyond reservoir surface area. G-res estimates of reservoir per-area greenhouse gas fluxes were quite variable, spanning more than three orders of magnitude (Range: 115–145,472 g CO_2 eq. m^{-2} y^{-1}). Highest per-area fluxes generally occurred near the equator and decreased at higher latitudes (Figure 3a). Further, the very highest per-area fluxes were driven primarily by CH_4 degassing, although ebullition fluxes were also quite substantial. For example, CH_4 degassing was the largest single flux pathway for GHG emissions in all of the top 10 GHG emitting reservoirs globally. The pattern where high fluxes occurred near the equator was not particularly surprising given G-res model structure (i.e., that effective temperature is an input parameter to G-res diffusive CO_2 and CH_4 sub-models), and is consistent with studies showing increasing CH_4 production rates with increasing temperatures (Barros et al., 2011; Thottathil et al., 2019; Yvon-Durocher et al., 2014), although see also Deemer et al. (2016) and Deemer and Holgerson (2021). In addition, annual fluxes tended to be lower at high latitudes due to the influence of freezing and the associated reduction of gas production. Although the pattern of decreasing fluxes with increasing latitude was unsurprising, an understanding of the magnitude of the latitude effect on per-area GHG fluxes is new. Further, the dominance of degassing and ebullition CH_4 fluxes throughout the tropics is a novel insight, deserving further investigation.

Similar to per-area fluxes, the highest GHG mass fluxes also occurred at low latitudes. 60.4% of total CH_4 emissions were estimated to occur between the Tropic of Cancer and the Tropic of Capricorn, and 75.2% of CH_4 emissions were estimated to occur within "tropical" climate zones, as defined by the IPCC (Rubel & Kottek, 2010). The tropical latitude band contained 14.9% of the reservoirs in our global database, while the subtropical band contained 22.7%. Despite some similarities in distribution between per-area GHG fluxes and GHG total mass fluxes, there were also some important differences, due to the uneven distribution of reservoir surface area by latitude (Compare Figures 3a and 3b). Mass fluxes of different gases exhibited different patterns with latitude, as did fluxes due to different CH_4 flux pathways (Table S3). CO_2 dominated fluxes at high northern latitudes (>63°N), accounting for 83% of total boreal reservoir GHG fluxes, whereas CH_4 accounted for almost half (48%) of the total greenhouse warming potential from reservoirs in temperate latitudes and the majority of total reservoir-sourced greenhouse warming potential in subtropical, and tropical latitudes (66.5% and 77.9%, respectively; Figure 3b). This latitudinal pattern results from the fact that CH_4 emissions (for CH_4 diffusion and, consequently, CH_4 degassing) tended to be depressed by low temperatures at high latitudes or (for ebullition) by low estimates of cumulative horizontal irradiance or low numbers of ice-free months. The relative contribution of bubbling is also variable among regions. In the boreal zone, CH_4 bubbling and degassing represented comparatively small fractions of total CH_4 fluxes

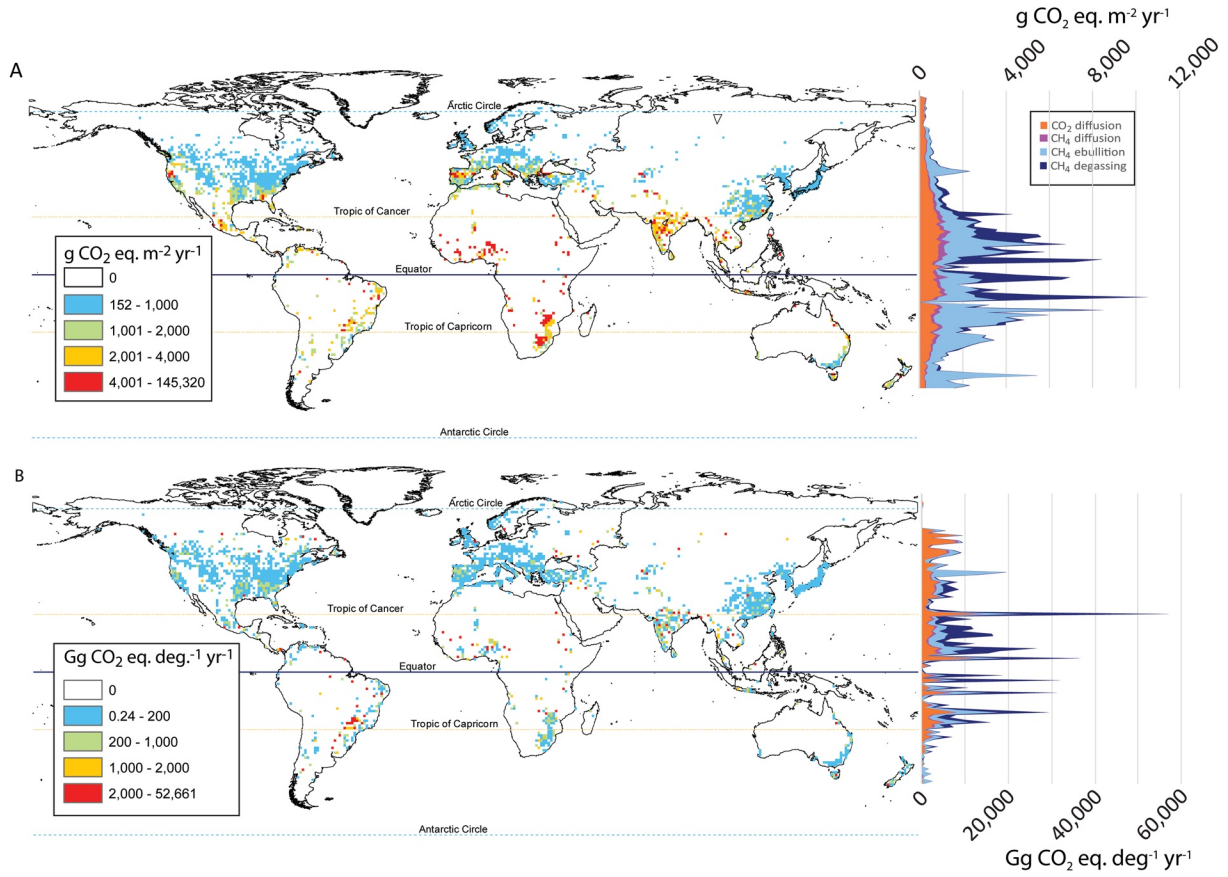

Figure 3. Global distribution and magnitudes of reservoir total (CH_4 + CO_2) GHG fluxes. Each one-degree grid-cell is color-coded according to G-res-predicted total CO_2 plus CH_4 flux from reservoirs in that cell. Panel A shows average per-reservoir-area rates of emissions (g CO_2 eq. m^{-2} yr^{-1}), with average per-reservoir-area fluxes for each 1-degree latitude band shown in the stacked line plot to the right (also g CO_2 eq. m^{-2} yr^{-1}). Panel B shows total mass fluxes of CH_4 + CO_2 GHG fluxes from reservoirs in each 1° × 1° grid cell (Gg CO_2 eq. $reservoir^{-1}$ yr^{-1}). Distribution of total mass flux by emission pathway and 1° latitude band is shown to the right of the map. In both panels, fluxes in the stacked line plots are additive such that in panel A the height of peaks represents average per-reservoir-area total flux per degree of latitude, while in panel B the height of the peaks represents the total reservoir-sourced GHG flux to the atmosphere for each 1° latitude band. White areas are regions lacking large reservoirs. Gridded model output available for download (Harrison et al., 2021).

(33.6% and 13.2%, respectively) whereas these flux pathways comprised a greater fraction of total CH_4 fluxes in temperate and tropical zones. Degassing was particularly important at tropical latitudes, accounting for 49% of all GHG fluxes (in CO_2 eq.) in that region. However, degassing accounted for a much smaller fraction of total GHG in the temperate zone (5.2%), where ebullition was a more important flux pathway, accounting for 38.5% of the GHG flux (in CO_2 eq.).

CH_4 degassing, CH_4 ebullition, and CO_2 diffusion were each the single largest GHG flux pathway for 287 (6.2%), 1,513 (33.2%), and 2,763 (60.6%) of the reservoirs in the G-res database, respectively, whereas CH_4 diffusion was never the dominant flux pathway in any reservoir (Figure 4). Hence, although CH_4 degassing constitutes a large portion of the global flux, this large flux is due to large per-area fluxes from a small fraction of reservoirs globally. In fact, according to G-res, the top 100 degassing reservoirs account for >90% of the global CH_4 degassing flux, and almost half (47%) of the global CH_4 degassing flux can be attributed to just 10 reservoirs. Although degassing fluxes have not been measured in most of these systems, CH_4 degassing fluxes have been measured in the reservoirs with the second and third highest predicted CH_4 degassing yields globally (Balbina and Tucurui reservoirs, respectively). In each case G-res-estimated CH_4 degassing flux was within a factor of two of direct measurement-based estimates. High degassing fluxes from a relatively small number of reservoirs, generally occurring at tropical latitudes, suggests that G-res predictions are sensitive to assumptions about which reservoirs contribute CH_4 to the atmosphere via this pathway. This highlights the need for both a broader empirical assessment of degassing emissions across a diversity

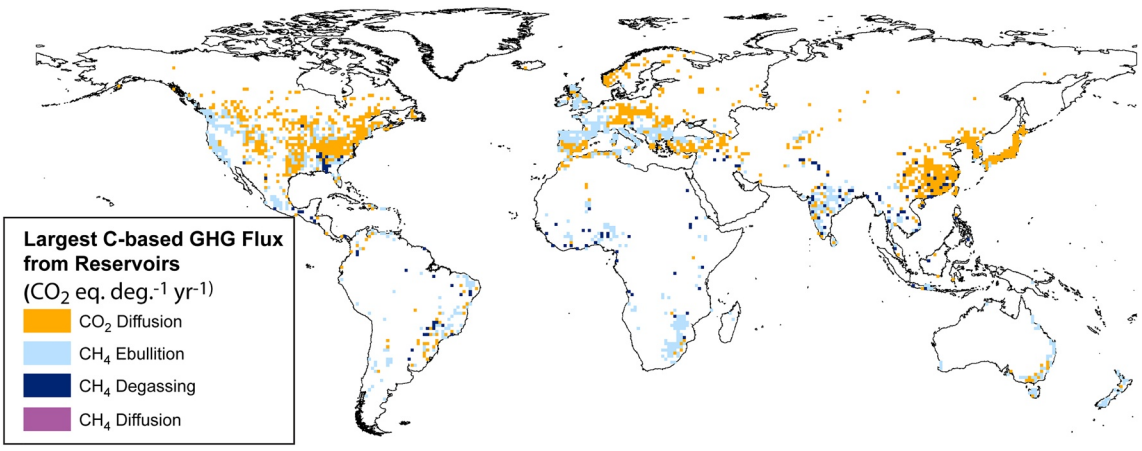

Figure 4. Dominant flux pathways for C-based greenhouse gases for each 1° × 1° grid cell. White areas are regions lacking large reservoirs.

of reservoirs, and more data on reservoir intake depth. Nevertheless, from a GHG mitigation perspective, the skewed distribution of reservoir degassing is intriguing in that it suggests that substantial reductions in CH_4 emissions via degassing may be possible by focusing mitigation efforts on a relatively small number of high-flux systems. In contrast to CH_4 degassing fluxes, which were limited to a relatively small subset of the global total number of reservoirs, CO_2 diffusion was the single largest flux from more than half of reservoirs in the G-res database, but these fluxes were on-average much smaller than degassing and ebullitive fluxes on a per-area CO_2 eq. basis. Focusing solely on CH_4 fluxes, a somewhat different picture emerges. In this case, CH_4 degassing CH_4 ebullition, and CH_4 diffusion, were the single largest CH_4 flux in 504 (11.0%), 3,338 (73.2%), 721 (15.8%) of G-res database reservoirs, respectively, highlighting the importance of ebullition as the largest CH_4 flux pathway in a majority of reservoirs. Dominant fluxes varied regionally in surprisingly consistent ways. Regions where ebullition was the single greatest GHG flux occurred in perennially ice-free regions with high rates of cumulative annual solar irradiance, consistent with observations in the few reservoirs where solar irradiance has been considered as a potential driver of CH_4 ebullition (Wik et al., 2014; Figure S3). In contrast, reservoir GHG fluxes in temperate regions with low cumulative annual solar irradiance tended to be dominated by CO_2 diffusion (Figure 4 and Figure S3). CO_2 diffusion also dominated GHG fluxes in north temperate and, especially, boreal regions. CO_2 diffusion was also the single largest GHG flux pathway throughout much of China, Japan, Korea, and the Eastern United States. In contrast, CH_4 ebullition tended to dominate GHG fluxes in the western United States, parts of Brazil, throughout much of southern Europe, in much of Africa, India, New Zealand, and western Australia. Degassing was only infrequently the dominant flux pathway regionally, but the regions where it was important included: the SE US, parts of Brazil, Eastern Europe, Central and Northern Africa (in the Nile River valley) as well as parts of both western and eastern China (Figure 4).

Importantly, the highest G-res-predicted per-area rates of emission occurred in exactly the regions where the majority of ongoing and planned new reservoir construction is anticipated to occur in coming decades: the developing tropics and subtropics (Zarfl et al., 2015). This suggests that dam construction could significantly increase global GHG fluxes from reservoir systems globally. Furthermore, the two largest estimated pathways for CH_4 emissions (ebullition and degassing) are also the most uncertain due to limited measurements (Tables 2 and 4) and comparatively unstable models (i.e., models that are sensitive to small changes in input parameters [see Section 3.4 below]). In the case of the degassing submodel, G-res estimates may be too low if hypolimnetic water release is more common than we estimate. Conversely G-res degassing estimates could be too high if hypolimnetic water release is less common or less constant (e.g., due to seasonal destratification) than estimated here. More work is required to better constrain these fluxes, both to improve understanding of aquatic C cycling and provide GHG management-relevant information. Similarly,

Table 4
G-res-Predicted Global, Year-2020 Fluxes of CH4 and CO2 by Flux Pathway

Flux pathway	(Tg CO_2 eq yr^{-1})
CH_4 diffusion	54 (42–77)
CH_4 ebullition	283 (184–660)
CH_4 degassing	411 (227–1,261)
CO_2 diffusion	328 (276–414)
Total (all flux pathways)	1,076 (730–2,412)

Table 5
G-res-Estimated Greenhouse Gas Fluxes by Climate Zone for Year-2020 Conditions

Climate zone	CH_4 and CO_2 ($Tg\ CO_2\ eq.\ yr^{-1}$)	% of total
Boreal	29.6	2.8
Cool temperate	107.6	10.0
Temperate warm/dry	61.4	5.7
Temperate warm/moist	67.7	6.3
Tropical dry/montane	350.1	32.5
Tropical moist/wet	456.4	42.4
Total Temperate	129.1	22.0
Total Tropical	806.5	75.0

Table 6
Results From a Model Efficiency Analysis Showing How Nash Sutcliffe Efficiency (NSE), an Indicator of Model Skill, Changes as a Function of Removal of Individual Model Components

Model parameter removed	Resulting NSE	Change in NSE from original model
No solar radiation (CH_4 ebullition)	−6.13	−6.71
No ice cover correction (CH_4 ebullition)	−6.13	−6.71
No temperature (CH_4 degassing)	−3.24	−4.08
No littoral area (CH_4 diffusion)	−0.36	−1.20
No littoral area (CH_4 degassing)	−0.26	−1.00
No temperature (CH_4 diffusion)	0.46	−0.38
No reservoir age (CO_2 diffusion)	0.58	−0.32
No littoral area (CH_4 ebullition)	0.30	−0.28
No temperature (CO_2 diffusion)	0.72	−0.17
No reservoir age (CH_4 diffusion)	0.69	−0.15
No water residence time (CH_4 degassing)	0.64	−0.10
No total P (CO_2 diffusion)	0.84	−0.05
No soil C content (CO_2 diffusion)	0.85	−0.04
No reservoir area (CO_2 diffusion)	0.87	−0.02

Notes. Model parameters where removal resulted in loss of little model skill (<0.38 NSE units) are shaded whereas parameters to which model skill was particularly sensitive are left unshaded.

G-res does not currently provide an estimate of CO_2 degassing. Although this component is likely small at the global scale, it may be significant in individual cases and should be further investigated.

3.4. Model Sensitivity, Efficiency, and Future Directions

3.4.1. Model Efficiency Analysis

An analysis of model efficiency, wherein model components are removed sequentially to evaluate the contribution of each to model predictive capacity, suggests that climate and geomorphological parameters are particularly important in determining G-res model skill (Table 6). In particular, the removal of the temperature-associated parameters (cumulative radiation and ice cover duration parameters) from the CH_4 ebullition model each substantially decreased G-res model skill, with the removal of each of these parameters from the model decreasing the NSE from 0.58 to to −6.13 (Tables 2 and 6). The removal of the temperature parameter from the CH_4 degassing model (not directly, but rather through its influence on the diffusive CH_4 model, which in-turn is an input to the CH_4 degassing model) substantially decreased that model's skill (NSE decreased from 0.74 to −3.24; Tables 2 and 5), and the removal of the temperature parameter from the CH_4 diffusion model decreased that G-res submodel's NSE from 0.84 to 0.46 (Tables 2 and 6). The temperature parameter in the CO_2 diffusion model had very little effect (decreased NSE value by only 0.17; Table 6), but the strong impact of the removal of temperature parameters on three out of the four G-res-estimated flux pathways suggests that temperature should be an important focus for attention and improvement in future iterations of the G-res model. The predictive skill of the G-res CH_4 ebullition and CH_4 diffusion submodels was also strongly dependent on the estimate of littoral area. Excluding the littoral area parameter from the CH_4 ebullition model decreased NSE from 0.58 to 0.30, and excluding the littoral area parameter from the CH_4 diffusion model decreased NSE from 0.84 to −0.36. In addition to its direct impact on CH_4 ebullition and CH_4 diffusion model skill, the littoral area parameter also affects the CH_4 degassing model through its impact on predicted CH_4 diffusion, which is a critical input to the CH_4 degassing model. Model skill for the CH_4 degassing submodel (NSE) decreased from 0.74 to −0.26 when the littoral area parameter was removed from the diffusive CH_4 flux model (Table 6). Because the littoral estimate strongly influences all three CH_4 flux pathways, which collectively account for about 70% of the global greenhouse gas liability due to reservoir emissions (CO_2 eq.), this is a very important parameter on which to focus energy in developing future iterations of the G-res model. The littoral area parameter is quite uncertain as it necessarily (due to a lack of better global scale data) relies on a simple algorithm estimating reservoir bathymetry as a function of average and maximum depth (See equations for "Littoral Fraction" and "Bathymetric Shape" in Table S1). Hence by improving estimates of this parameter, for example by using better reservoir geomorphology information, future iterations of G-res may improve substantially. In contrast to temperature-related and geomorphometric parameters, G-res model skill was relatively robust to removal of other input parameters such as reservoir age, water residence time, soil C content, total P loading, and reservoir surface area. In each case, parameter removal reduced model NSE by less than 0.32 units, and often far less (Table 6).

3.4.2. Model Sensitivity Analysis

A sensitivity analysis in which G-res model inputs and coefficients were increased by 10% in order to evaluate model response (Table 7) was

Table 7
Results of a Model Sensitivity Analysis Showing G-res Predictions of Total Global Reservoir GHG Flux Change as a Function of a 10% Increase in Various Model Drivers

Model parameter modified	% Change in G-res-predicted global $CO_2 + CH_4$ emissions resulting from a 10% Increase in input parameter values (g CO_2 eq. yr^{-1})
Littoral area fraction	**191.1**
Effective temperature	**60.9**
Solar radiation	**33.7**
Ice-free period	**33.7**
Reservoir surface area	**10.1**
Actual age plus 10 years	−3.6
Water residence time	2.4
Total P	2.5
Inundated soil C content	0.8

Notes. Values in bold are greater than 10%, indicating the G-res model is comparatively sensitive to changes in the associated input parameters.

consistent with the efficiency analysis in that it suggested that G-res model predictions are sensitive to small changes in temperature- and geomorphology-related parameters but comparatively insensitive to changes in other parameters. The overall model was quite insensitive to 10% increases in the C content of inundated soils, total P content, and reservoir age, with model predictions changing far less than 10% in each case. As expected, based on the model formulation, predicted fluxes scale approximately linearly with reservoir surface area. In contrast, but consistent with the results of the efficiency analysis described above, G-res predictions were very sensitive to small (10%) increases in (and hence to small errors in estimates of) littoral area fraction in reservoirs, increasing more than 11-fold. G-res predictions were also quite sensitive to changes in temperature-related parameters, including effective temperature, cumulative radiation, and the length of the ice-free season. As with the littoral area parameter, there is also room for improvement in the temperature-related parameters. At the global scale there is not currently a global water temperature database for reservoirs; nor is there a widely accepted method to reliably and accurately link sediment and water column temperatures to air temperatures. Any enhancements inability to model water temperatures at large scales is likely to enhance understanding of regional and global reservoir GHG fluxes.

3.4.3. Future Directions

Taken together, results from efficiency and sensitivity analyses suggest that littoral area and temperature are two major sources of G-res model uncertainty, and hence opportunities for model enhancement. Work to link air temperatures to water temperatures (esp. bottom-water temperatures) and improve estimates of lake bathymetry and stratification dynamics at large scales would both be useful. These two parameters are also changing with a changing climate (Kraemer et al., 2015; O'Reilly et al., 2015) and likely to change further in coming decades in manners that are likely to accelerate reservoir GHG emissions (i.e., higher temperatures, deeper thermoclines; Woolway et al., 2020), highlighting a need to study, monitor, and improve methods for estimating changing water temperatures and stratification regimes.

In addition to better constraining temperature and geomorphometric model input parameters, there are some additional model improvements that should be considered in future iterations of regional and global lake and reservoir GHG emissions models. One of these improvements is the inclusion of an explicit trophic status or primary production parameter. Several recent studies have reported strong correlations between primary production and CH_4 emissions (Beaulieu et al., 2019; Deemer et al., 2016; DelSontro et al., 2018; Harrison et al., 2017), and there is good reason to think there is a causal link between primary production and CH_4 emission. By providing organic C and creating the anoxic conditions that favor CH_4 production, biological production in surface waters is likely to fuel higher rates of CH_4 emission, leading to higher emissions from eutrophic systems than oligotrophic systems. To some extent, G-res models use cumulative radiance and total phosphorus concentrations as indirect and imperfect proxies for primary productivity. Yet, no large-scale models, including G-res, currently include a primary production term as a model input. This is because there are no global datasets of lake or reservoir primary productivity that are sufficiently robust to be of use for this application. However, work is ongoing in this area (Sayers et al., 2015), and this is likely to change within the next several years. Another area meriting additional investigation is understanding how global reservoir GHG emissions will change in the future with the ongoing and anticipated global boom in reservoir impoundment (Zarfl et al., 2015).

4. Conclusion

Despite remaining uncertainties and opportunities for further improvement, the work presented here represents a significant step forward in understanding and representing global and regional reservoir GHG fluxes. Here we present the first-ever spatially and temporally explicit, global estimates of reservoir CO_2 and CH_4 fluxes modeled for individual reservoirs and not simply based on the product of mean flux rates and reservoir surface area. In addition, we present a first-ever spatially explicit estimate of the global reservoir CH_4 degassing flux. Analysis of these novel results grants several important new insights including the following: (a) diffusive CH_4 fluxes are probably lower than has previously been estimated; (b) CH_4 fluxes via ebullition and degassing are larger than previously recognized, but also quite poorly constrained; (c) these fluxes are highest in the tropics and subtropics, which, together, are expected to account for 65%–75% of new hydropower dam construction and reservoir impoundment in coming decades (Zarfl et al., 2015); (d) global distribution of emissions shows that the contribution of CO_2 flux is the most important in boreal climate while CH_4 degassing and ebullition contribution is dominant in tropical and subtropical climate; and (e) G-res estimated reservoir GHG fluxes are quite sensitive to input parameters that are both poorly constrained and likely to be strongly influenced by climate change in coming decades. Together these results highlight a critical need both to better understand climate-related drivers of GHG emission and the relationship between these drivers and the highly uncertain CH_4 ebullition and degassing fluxes.

Data Availability Statement

Datasets and model output for this research are available in these in-text data citation references: Harrison et al. (2021), and Prairie et al. (2021).

Acknowledgments
We thank Atle Harby, Jukka Alm, Sofia D'Ambrosio, and Stephen Henderson for input on early drafts of this manuscript. Funding to JAH was provided by an NSF INFEWS grant (NSF EAR1639458), a GRIL Fellowship grant, the Cox visiting professorship fund at Stanford University, a U.S. Army Corps of Engineers Climate Preparedness and Resilience Programs grant, and a NSF DEB Grant #1355211. Financial support to YTP and SMB was provided by the International Hydropower Association for the development of the G-res models.

References

Abril, G., Guérin, F., Richard, S., Delmas, R., Galy-Lacaux, C., Gosse, P., et al. (2005). Carbon dioxide and methane emissions and the carbon budget of a 10-year old tropical reservoir (Petit Saut, French Guiana). *Global Biogeochemical Cycles*, *19*(4). https://doi.org/10.1029/2005GB002457

Barros, N., Cole, J. J., Tranvik, L. J., Prairie, Y. T., Bastviken, D., Huszar, V. L. M., et al. (2011). Carbon emission from hydroelectric reservoirs linked to reservoir age and latitude. *Nature Geoscience*, *4*(9), 593–596. https://doi.org/10.1038/ngeo1211

Bastviken, D., Tranvik, L. J., Downing, J. A., Crill, P. M., & Enrich-Prast, A. (2011). Freshwater methane emissions offset the continental carbon sink. *Science*, *331*, 50. https://doi.org/10.1126/science.1196808

Beaulieu, J. J., DelSontro, T., & Downing, J. A. (2019). Eutrophication will increase methane emissions from lakes and impoundments during the 21st century. *Nature Communications*, *10*. https://doi.org/10.1038/s41467-019-09100-5

Butman, D., & Raymond, P. A. (2011). Significant efflux of carbon dioxide from streams and rivers in the United States. *Nature Geoscience*. Retrieved from http://www.nature.com/ngeo/journal/vaop/ncurrent/abs/ngeo1294.html

Cole, J. J., Prairie, Y. T., Caraco, N. F., McDowell, W. H., Tranvik, L. J., Striegl, R. G., et al. (2007). Plumbing the global carbon cycle: Integrating inland waters into the terrestrial carbon budget. *Ecosystems*, *10*, 172–185. https://doi.org/10.1007/s10021-006-9013-8

Deemer, B. R., Harrison, J. A., Li, S., Beaulieu, J. J., Delsontro, T., Barros, N., et al. (2016). Greenhouse gas emissions from reservoir water surfaces: A new global synthesis. *BioScience*, *66*, 949–964. https://doi.org/10.1093/biosci/biw117

Deemer, B. R., & Holgerson, M. A. (2021). Drivers of methane flux differ between lakes and reservoirs, complicating global upscaling efforts. *Journal of Geophysical Research: Biogeosciences*, *126*. https://doi.org/10.1029/2019JG005600

DelSontro, T., Beaulieu, J. J., & Downing, J. A. (2018). Greenhouse gas emissions from lakes and impoundments: Upscaling in the face of global change. *Limnology and Oceanography Letters*, *3*(3), 64–75. https://doi.org/10.1002/lol2.10073

Downing, J. A., Prairie, Y. T., Cole, J. J., Duarte, C. M., Tranvik, L. J., Striegl, R. G., et al. (2006). The global abundance and size distribution of lakes, ponds, and impoundments. *Limnology & Oceanography*, *51*(5), 2388–2397. https://doi.org/10.4319/lo.2006.51.5.2388

Harrison, J. A., Deemer, B. R., Birchfield, M. K., & O'Malley, M. T. (2017). Reservoir water-level drawdowns accelerate and amplify methane emission. *Environmental Science and Technology*, *51*(3), 1267–1277. https://doi.org/10.1021/acs.est.6b03185

Harrison, J. A., Prairie, Y. T., Mercier-Blais, S., & Soued, C. (2021). Year 2020 reservoir methane and CO_2 emissions as predicted by the g-res model. *Zenodo*. https://doi.org/10.5281/zenodo.4632428

Hertwich, E. G. (2013). Addressing biogenic greenhouse gas emissions from hydropower in LCA. *Environmental Science and Technology*, *47*(17), 9604–9611. https://doi.org/10.1021/es401820p

Inglett, K. S., Inglett, P. W., Reddy, K. R., & Osborne, T. Z. (2012). Temperature sensitivity of greenhouse gas production in wetland soils of different vegetation. *Biogeochemistry*, *108*(1–3), 77–90. https://doi.org/10.1007/s10533-011-9573-3

Kraemer, B. M., Anneville, O., Chandra, S., Dix, M., Kuusisto, E., Livingstone, D. M., et al. (2015). Morphometry and average temperature affect lake stratification responses to climate change. *Geophysical Research Letters*, *42*, 4981–4988. https://doi.org/10.1002/2015GL064097

Lehner, B., Reidy Liermann, C., Revenga, C., Vorosmarty, C., Fekete, B., Crouzet, P., et al. (2011). *Global reservoir and dam database, version 1 (GRanDv1): Dams, revision 01*. NASA Socioeconomic Data and Applications Center (SEDAC). https://doi.org/10.7927/H4N877QK

Maavara, T., Chen, Q., Van Meter, K., Brown, L. E., Zhang, J., Ni, J., & Zarfl, C. (2020). River dam impacts on biogeochemical cycling. *Nature Reviews Earth & Environment*, *1*, 103–116. https://doi.org/10.1038/s43017-019-0019-0

Maavara, T., Lauerwald, R., Regnier, P., & Van Cappellen, P. (2017). Global perturbation of organic carbon cycling by river damming. *Nature Communications*, *8*. https://doi.org/10.1038/ncomms15347

Michie, L. E., Hitchcock, J. N., Thiem, J. D., Boys, C. A., & Mitrovic, S. M. (2020). The effect of varied dam release mechanisms and storage volume on downstream river thermal regimes. *Limnologica*, *81*, 125760. https://doi.org/10.1016/j.limno.2020.125760

Nash, E., & Sutcliffe, V. (1970). Part I-A discussion of principles. *Journal of Hydrology*, *10*, 282–290. https://doi.org/10.1016/0022-1694(70)90255-6

Newman, M. C. (1993). Regression analysis of log-transformed data: Statistical bias and its correction. *Environmental Toxicology & Chemistry*, *12*, 1129–1133. https://doi.org/10.1002/etc.5620120618

O'Reilly, C. M., Sharma, S., Gray, D. K., Hampton, S. E., Read, J. S., Rowley, R. J., et al. (2015). Rapid and highly variable warming of lake surface waters around the globe. *Geophysical Research Letters*. https://doi.org/10.1002/2015GL066235

Prairie, Y. T., Alm, J., Beaulieu, J., Barros, N., Battin, T., Cole, J., et al. (2018). Greenhouse gas emissions from freshwater reservoirs: What does the atmosphere see? *Ecosystems*, *21*(5). https://doi.org/10.1007/s10021-017-0198-9

Prairie, Y. T., Alm, J., Harby, A., Mercier-Blais, S., & Nahas, R. (2017). *Technical documentation, UNESCO/IHA research project on the GHG status of freshwater reservoirs. Version 1.1*. https://www.hydropower.org/publications/the-ghg-reservoir-tool-g-res-technical-documentation

Prairie, Y. T., Mercier-Blais, S., Harrison, J. A., Soued, C., del Giorgio, P., Harby, A., et al. (2021). G-res tool modelling database. *Zenodo*. https://doi.org/10.5281/zenodo.4711132

Raymond, P. A., Hartmann, J., Lauerwald, R., Sobek, S., McDonald, C., Hoover, M., et al. (2013). Global carbon dioxide emissions from inland waters. *Nature*, *503*(7476), 355–359. https://doi.org/10.1038/nature12760

Rosentreter, J. A., Borges, A. V., Deemer, B. R., Holgerson, M. A., Liu, S., Song, C., et al. (2021). Aquatic ecosystems are highly variable sources contributing half of the global methane emissions. *Nature Geoscience*. https://doi.org/10.1038/s41561-021-00715-2

Rubel, F., & Kottek, M. (2010). Observed and projected climate shifts 1901—2100 depicted by world maps of the Koppen-Geiger climate classification. *Meteorologische Zeitschrift*, *19*(2), 135–141. https://doi.org/10.1127/0941-2948/2010/0430

Saunois, M., Stavert, A. R., Poulter, B., Bousquet, P., Canadell, J. G., Jackson, R. B., et al. (2020). The global methane budget 2000-2017. *Earth System Science Data*, *12*, 1561–1623. https://doi.org/10.5194/essd-12-1561-2020

Sayers, M. J., Grimm, A. G., Shuchman, R. A., Deines, A. M., Bunnell, D. B., Raymer, Z. B., et al. (2015). A new method to generate a high-resolution global distribution map of lake chlorophyll. *International Journal of Remote Sensing*, *36*(7), 1942–1964. https://doi.org/10.1080/01431161.2015.1029099

Soued, C., & Prairie, Y. T. (2020). The carbon footprint of a Malaysian tropical reservoir: Measured versus modeled estimates highlight the underestimated key role of downstream processes. *Biogeosciences*, *30*(October), 1–22. https://doi.org/10.5194/bg-2019-385

St Louis, V. L., Kelly, C. A., Duchemin, É., Rudd, J. W. M., & Rosenberg, D. M. (2000). Reservoir surfaces as sources of greenhouse gases to the atmosphere: A global estimate. *BioScience*, *50*(9), 766–775. https://doi.org/10.1641/0006-3568(2000)050[0766:RSASOG]2.0.CO;2

Teodoru, C. R., Bastien, J., Bonneville, M.-C. C., del Giorgio, P. A., Demarty, M., Garneau, M., et al. (2012). The net carbon footprint of a newly created boreal hydroelectric reservoir. *Global Biogeochemical Cycles*, *26*(2). https://doi.org/10.1029/2011GB004187

Thottathil, S. D., Reis, P. C. J., & Prairie, Y. T. (2019). Methane oxidation kinetics in northern freshwater lakes. *Biogeochemistry*, *143*(1), 105–116. https://doi.org/10.1007/s10533-019-00552-x

Tranvik, L., Downing, J., Cotner, J., Loiselle, S., Striegl, R., Ballatore, T., et al. (2009). Lakes and reservoirs as regulators of carbon cycling and climate. *Limnology & Oceanography*, *54*(6), 2298–2314. https://doi.org/10.4319/lo.2009.54.6_part_2.2298

Wik, M., Crill, P. M., Varner, R. K., & Bastviken, D. (2013). Multiyear measurements of ebullitive methane flux from three subarctic lakes. *Journal of Geophysical Research: Biogeosciences*, *118*(3), 1307–1321. https://doi.org/10.1002/Jgrg.20103

Wik, M., Thornton, B. F., Bastviken, D., MacIntyre, S., Varner, R. K., & Crill, P. M. (2014). Energy input is primary controller of methane bubbling in subarctic lakes. *Geophysical Research Letters*, *41*(2), 555–560. https://doi.org/10.1002/2013gl058510

Wik, M., Thornton, B. F., Bastviken, D., Uhlback, J., Crill, P. M., Uhlbäck, J., et al. (2016). Biased sampling of methane release from northern lakes: A problem for extrapolation. *Geophysical Research Letters*, *43*(3), 1256–1262. https://doi.org/10.1002/2015gl066501

Woolway, R. I., Kraemer, B. M., Lenters, J. D., Merchant, C. J., O'Reilly, C. M., & Sharma, S. (2020). Global lake responses to climate change. *Nature Reviews Earth & Environment*, *1*, 388–403. https://doi.org/10.1038/s43017-020-0067-5

Yvon-Durocher, G., Allen, A. P., Bastviken, D., Conrad, R., Gudasz, C., St-Pierre, A., et al. (2014). Methane fluxes show consistent temperature dependence across microbial to ecosystem scales. *Nature*, *507*(7493), 488–491. https://doi.org/10.1038/nature13164

Zarfl, C., Lumsdon, A. E., Berlekamp, J., Tydecks, L., & Tockner, K. (2015). A global boom in hydropower dam construction. *Aquatic Sciences*, *77*(1), 161–170. https://doi.org/10.1007/s00027-014-0377-0